Supplementary Material

Deliquescence, Efflorescence, and Phase Miscibility of Mixed Particles of Ammonium Sulfate and Isoprene-Derived Secondary Organic Material

M.L. Smith, A.K Bertram, and S.T. Martin

Equation	Experiment Label	$d_{m,+1}^{mono}$	$d_{m,+1}^{filter}$	Arm	RH^{CMFR}	RH^{mono}	RH_1^{nafion}	RH_2^{nafion}	Measurement
n/a	Deliquescence: Reference Arm	{75,120}	$d_{m,+1}^{mono}$	α	40	60	60	60	$\frac{N_\beta^{filter}}{N_\alpha^{filter}}$
1	Deliquescence: Test Arm	{75,120}	$d_{m,+1}^{mono}$	β	40	60	*x*:60→90	60	
n/a	Efflorescence: Reference Arm	{90*,120*}	$d_{m,+1}^{mono}$	α	40	50	50	50	$\frac{N_\beta^{filter}}{N_\alpha^{filter}}$
2	Efflorescence: Test Arm	{90*,120*}	$d_{m,+1}^{mono}$	β	40	50	*x*:50→15	50	
3A	Hygroscopic Test for Deliquescence	{75,190}	scanned	β	40	7	*x*:10→85	*x*:10→85	$N(d)$
3B	Hygroscopic Control for forced Deliquescence	{75,190}	scanned	β	40	7	90	*x*:10→85	$N(d)$
5A	Hygroscopic Test for Efflorescence at 7%	{75,150}	scanned	β	40	7	50	50	$N(d)$
5B	Hygroscopic Test for Efflorescence at 7%	{75,150}	scanned	β	40	7	90	50	$N(d)$
n/a	Hygroscopic Test for Efflorescence - perturbation	{90*,120*}	scanned	β	40	50	*x*:50→9	50	$N(d)$

Table S1. List of experimental modes of TDMA operation and relative humidity cycles used to determine DRH(ε) and ERH(ε) from transmission ratio (rows 1-4) and number-diameter distribution experiments (rows 5-9). For simplicity, adjacent RH values that are equal are condensed to a single RH value in the table. An asterisk (*) indicates that the classified particle was on the upper branch of the hysteresis curve.

$N_{3B}(d,y)$ compared to $N_{3A}(d,y)$ is…	DRH(ε) > 40%	ERH(ε) > 7%	DRH(ε) > y	ERH(ε) > y
n/a	True	True	True	**True**
shifted right	True	True	True	False
n/a	True	True	False	**True**
identical	True	True	False	False
n/a	True	False	True	**True**
shifted right	True	False	True	False
n/a	True	False	False	**True**
identical	True	False	False	False
n/a	False	True	True	**True**
n/a	**False**	True	**True**	False
n/a	False	True	False	**True**
identical	False	True	False	False
n/a	False	False	True	**True**
n/a	**False**	False	**True**	False
n/a	False	False	False	**True**
identical	False	False	False	False

Table S2. Evaluation of the 16 possible outcomes of the comparison of $N(d,y;\varepsilon)$ of Eq. (3A) to that of $N(d,y;\varepsilon)$ of Eq. (3B) based on whether the following conditions are true: DRH(ε) > 40%, ERH(ε) > 7%, DRH(ε) > y, and ERH(ε) > y. The entry "n/a" indicates a condition that, based on inference from the results of the transmission ratio experiments as summarized in Fig. 4, is never satisfied for this data set for $y \geq 40\%$. Bolded entries show the conditions that lead to "n/a".

$N_{3B}(d,y)$ compared to $N_{3A}(d,y)$ is…	DRH(ε) > 40%	ERH(ε) > 7%	DRH(ε) > y	ERH(ε) > y
shifted right	True	n/a	True	n/a
identical	True	n/a	False	n/a
identical	False	n/a	n/a	n/a

Table S3. Condensed results of the analysis in Table S2 following removal of "n/a" entries and logically identical elements. This table appears as Eq. (4) in the main text, with the substitution of DRH(ε) > 40% by $\varepsilon < \varepsilon_D(40\%)$.

List of Figures

Figure S1. Examples of the number-diameter distributions of the ammonium sulfate seed particles in the CMFR inflow (solid lines) and of the number-diameter distributions of the mixed organic-inorganic particles in the CMFR outflow (dotted lines). The distributions are scaled to a height of unity so that the features of the particle population exiting the chamber can be clearly seen. The two shown distributions were collected 10 months apart, demonstrating consistency of the experimental conditions.

Figure S2. Optimal value of RH^{mono} for transmission ratio experiments. For both deliquescence- and efflorescence-mode experiments, the optimal value of RH^{mono} satisfies $g = 1.12$ while maximizing ε. The line of $g = 1.12$ is drawn in green. The DRH(ε) curve of this study, as parameterized in Table 1, is drawn in blue. The intersection of the green line with the blue line is the optimal value for RH^{mono}. This value is 69.5% and corresponds to $\varepsilon_D(69.5\%) = 0.66$. Higher values of ε can be probed through the number-diameter distribution experiments.

As further explanation, horizontal red lines labeled 1, 2, and 3 are drawn at $RH^{mono} = 69.5\%$ and at values above and below RH^{mono}. The solid portion of the red line corresponds to $g > 1.12$ so that the transmission ratio experiments can be carried out. The dashed portion of the red line corresponds to $g < 1.12$ so that full size separation is not achieved between DMA^{mono} and DMA_{β}^{filter}.

Lines 1, 2, and 3 demonstrate that RH^{mono} is the optimal value to maximize the experimental range of ε that can be studied in the transmission ratio experiments. For line 1 compared to

line 2, transmission ratio experiments are possible for the full range of ε but $\varepsilon_2 > \varepsilon_1$. For line 3 compared to line 2, transmission ratio experiments are no longer possible once line 3 intersects the line of $g = 1.12$. In this case, $\varepsilon_2 > \varepsilon_3$. The value of ε_2 therefore represents the maximum value.

As a technical note, the value of g required for complete separation between DMA^{mono} and $\mathrm{DMA}_{\beta}^{filter}$ increases for increasing setpoint diameter because the width of the DMA transfer function broadens. The stated value of 1.12 holds for a setpoint diameter of 100 nm.

Figure S3. Additional examples of (A) DRH(ε) curves derived from transmission ratio experiments and (B) associated modeled cumulative distribution functions $P(\varepsilon)$ of organic volume fraction. The vertical dashed line shows the condition $g = 1.12$. The DRH(ε) curves are consistent with one another despite the large differences in underlying $P(\varepsilon)$ among the three experiments. This consistency indicates high confidence in the data analysis.

Figure S4. Modeling hygroscopic growth and phase transitions for number-diameter distribution experiments (Eq. (3A)). Columns correspond to the progressive steps of RH history represented by Eq. (3A). Rows represent particle types A, B, C, and D (cf. Section 3.1). The heavy colored lines in column 3 correspond to the same colored lines shown in Fig. 3A. The sum of these lines is the modeled size distribution for the entire particle population and appears as the red dashed line of Fig. 3A.

For clarity of presentation, the distributions in Fig. S4 are represented by discretized bars, and the bar widths are shown at increased coarseness compared to the actual model. The

gradient of bar shading represents the fraction *f* of ammonium sulfate that is dissolved, as follows: (1) the scale bar is shown in uniform gradient from 0.0 to 1.0 in ten equally sized height steps and (2) the gradient in height steps at one diameter in one panel represents the relative fraction of particles having that value of *f*. For instance, for particle type A at 40% RH, the bar at 90 nm shows that most particles are characterized by $0.0 \leq f < 0.1$, followed by some particles of $0.1 \leq f < 0.2$. By comparison, at 7% RH all particles have $0.0 \leq f < 0.1$. Particles that are of $f = 1$, indicating that they are on the upper side of the hysteresis loop, are represented by red shading. The heterogeneity in particle water content at different diameters and RH, shown by the shading of *f*, demonstrates the need for a hygroscopic model that incorporates the distribution of *f* and the corresponding diameter growth to aid in the interpretation of data sets such as those represented in Fig. 3A.

In regard to column 1, a further note of explanation is that the shown distributions represent a subset of the polydisperse distribution that exits the CMFR. This subset corresponds to those particles that are subsequently selected by DMA^{mono} set to $d_{m,+1}^{mono} = 90$ nm at 7% RH (Eq. (3A)). Column 1 illustrates the phase state of the relevant particle sub-population in the CMFR outflow.

Figure S5. Correction made in the analysis for particle water content. Particles selected by DMA^{mono} for RH ≥ 50% contain non-negligible volumes of water; water-free distributions are needed to calculate $P(\varepsilon)$. An iterative optimization approach is used for estimating the dry number-diameter distribution, as follows: (1) a dry number-diameter distribution is assumed (panel A), (2) a model of hygroscopic growth is applied to the dry distribution (cf. Appendix of main text), and (3) the modeled distribution is compared to the distribution that is implied

by the transfer function of DMA^{mono} (panel B). These steps are repeated iteratively by refining the assumed dry number-diameter distribution until the modeled distribution converges to the implied distribution. Particle types A (blue), B (pink), and D (orange) are modeled separately. The cumulative distribution function given by $P(\varepsilon) = \sum_T p(\varepsilon;T)$ appears in Figure 2B.

Figure S6. Hygroscopic diameter growth factors. (blue) The growth factor g_0 of ammonium sulfate on the upper branch of the hysteresis curve is from Biskos et al. (2006). (red) The growth factor is unity for ammonium sulfate on the lower branch of the hysteresis curve. (green) The growth factor g_1 of isoprene-derived SOM is parameterized as $g_1(y) = 1 + (1-y)^{-A} B y^C$ for A = 0.1683, B = 0.1768, C = 2.600, and y = RH/100 for the data set shown in the inset for $0.0 < y < 0.9$. Horizontal dotted lines show the DRH and ERH of pure ammonium sulfate.

Figure S7. Sensitivity of (A) $f(\varepsilon)$ and (B) $p(d_{m,+1})$ to the value of parameter ε_D. The inset shows the sum of the squares of the differences between model predictions (lines) and data points (squares) for the different values of ε_D from 0.70 to 0.92. The specific values of ε_D for the lines correspond to the points shown in the inset (i.e., values of ε_D are more closely sampled near the minimum than away from it). In panels A and B, lines are colored from red (good fit) to blue (poor fit). The color bar is shown along the ordinate of the inset.

References

Biskos, G., Paulsen, D., Russell, L. M., Buseck, P. R. and Martin, S. T.: Prompt deliquescence and efflorescence of aerosol nanoparticles, Atmos. Chem. Phys., 6, 4633-4642, 2006.

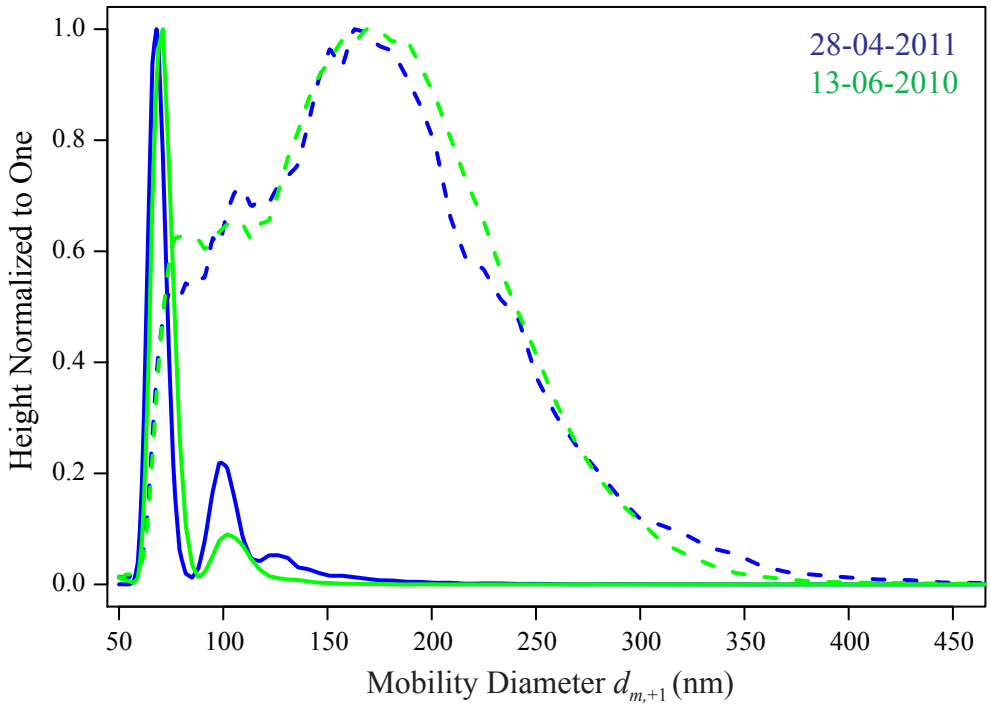
28-04-2011
13-06-2010
Height Normalized to One
1.0
0.8
0.6
0.4
0.2
0.0
50
100
150
200
250
300
350
400
450
Mobility Diameter $d_{m,+1}$ (nm)

Figure S1

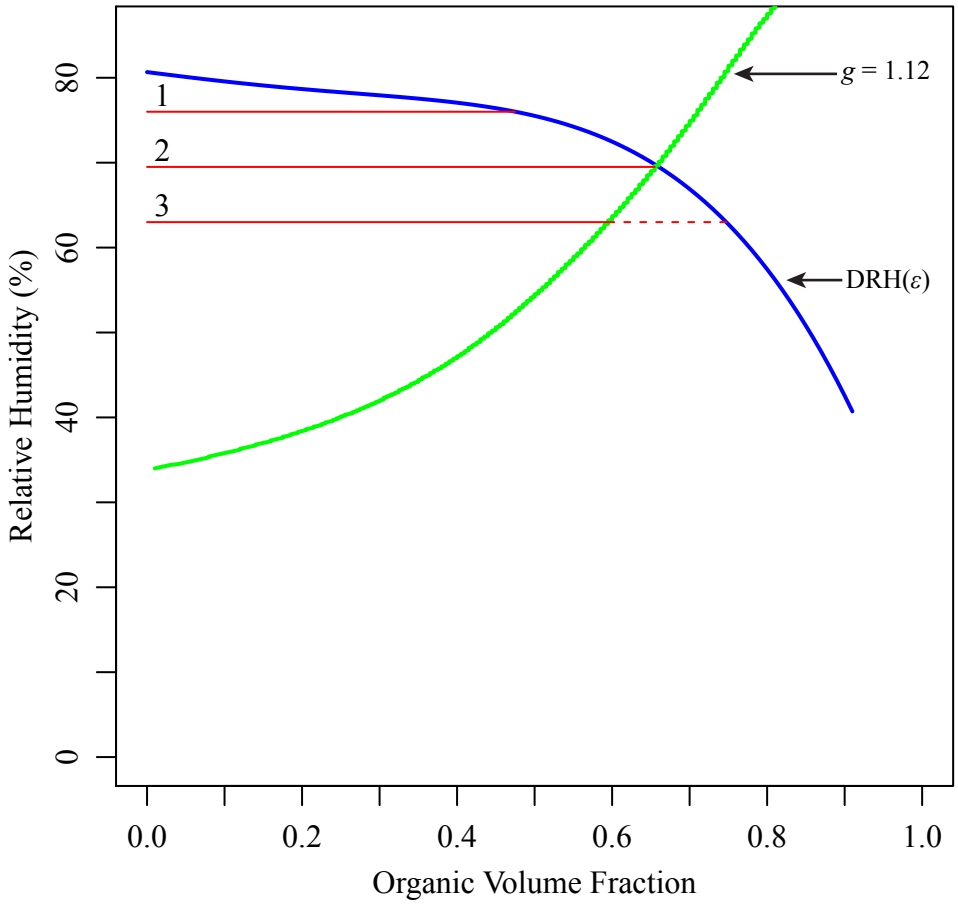
Relative Humidity (%)
0
20
40
60
80
0.0
0.2
0.4
0.6
0.8
1.0
Organic Volume Fraction
1
2
3
g = 1.12
DRH(ε)

Figure S2

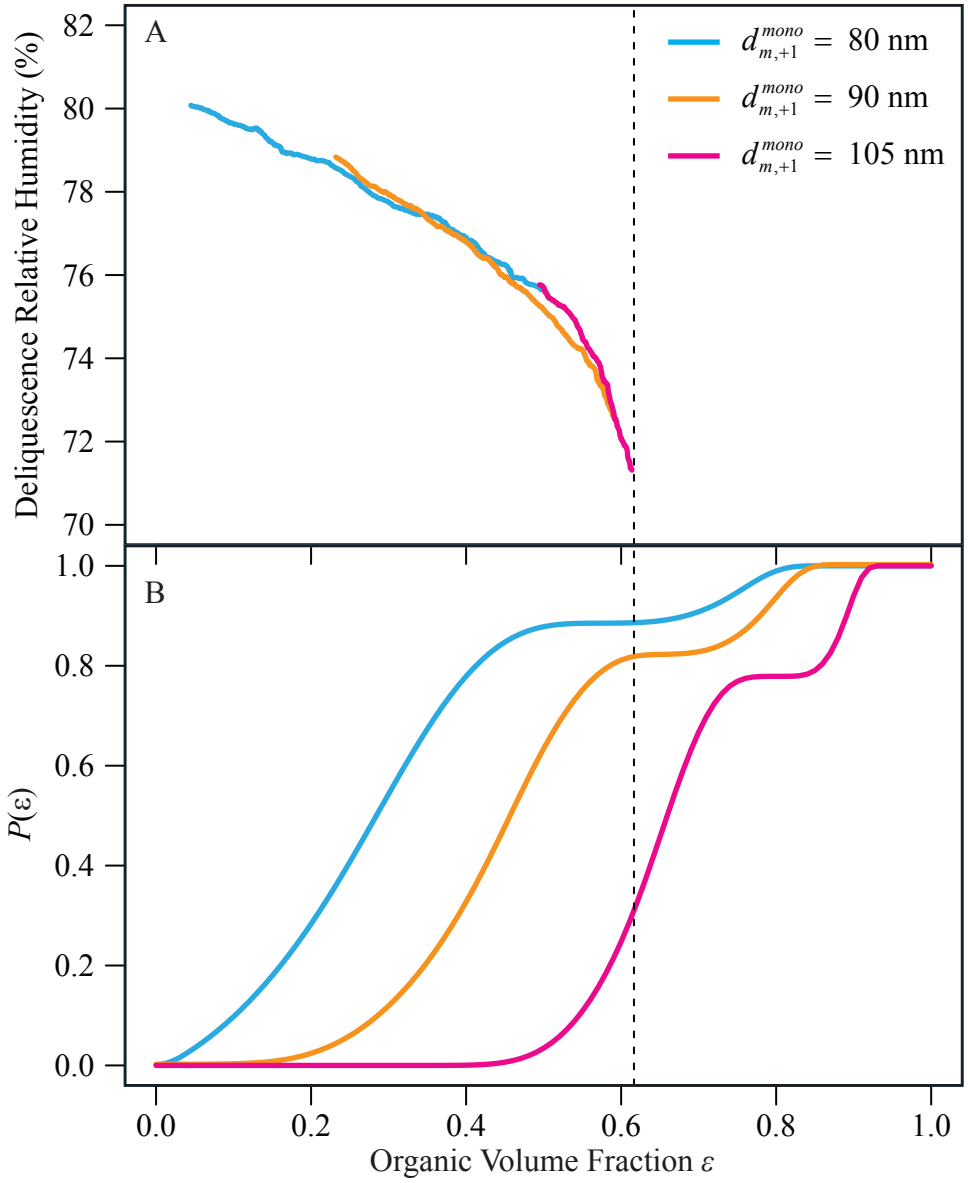
A
B
Deliquescence Relative Humidity (%)
82
80
78
76
74
72
70
$d^{mono}_{m,+1}$ = 80 nm
$d^{mono}_{m,+1}$ = 90 nm
$d^{mono}_{m,+1}$ = 105 nm
P(ε)
1.0
0.8
0.6
0.4
0.2
0.0
0.0
0.2
0.4
0.6
0.8
1.0
Organic Volume Fraction ε

Figure S3

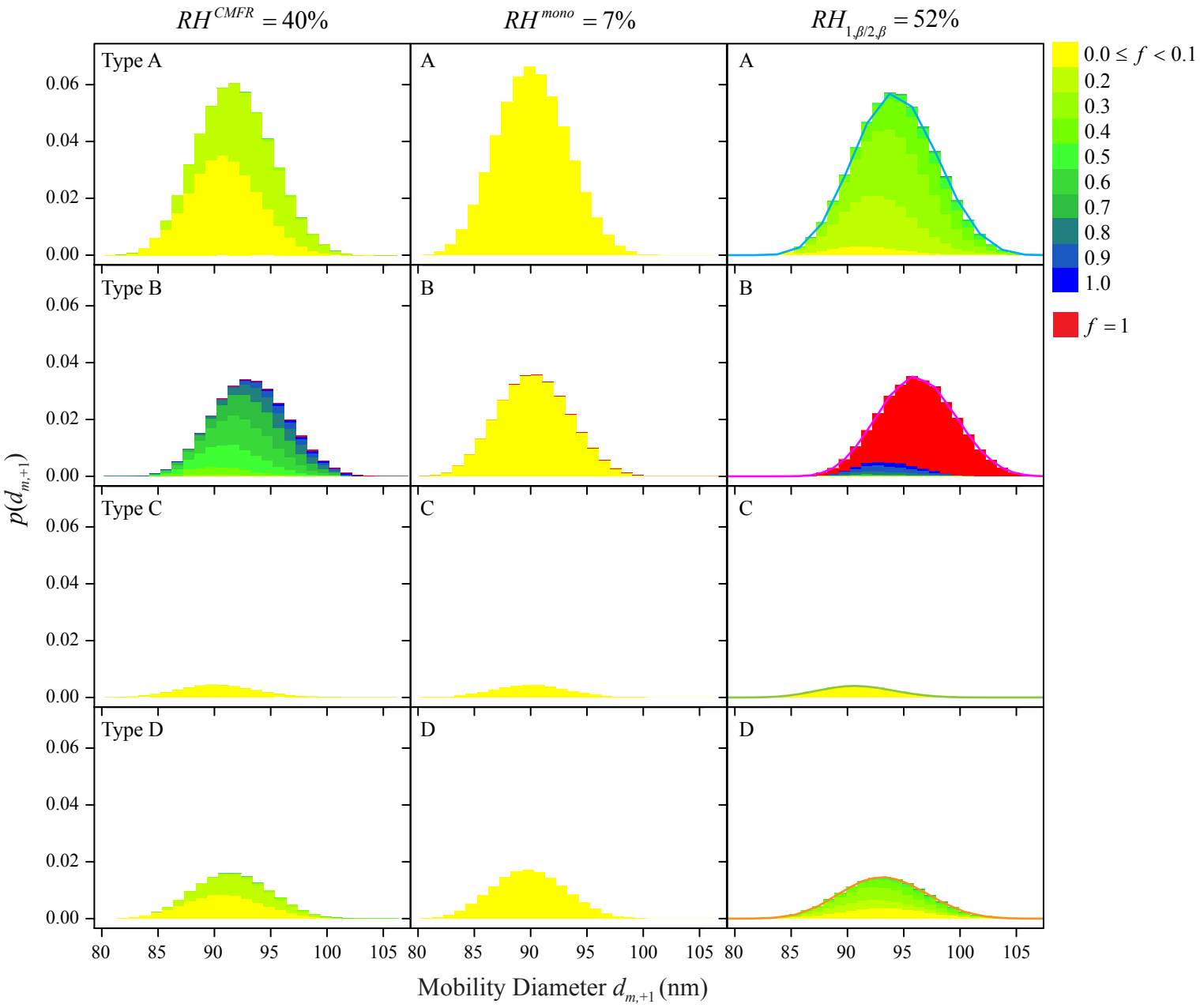
$RH^{CMFR} = 40\%$
$RH^{mono} = 7\%$
$RH_{1,\beta/2,\beta} = 52\%$
Type A
Type B
Type C
Type D
A
B
C
D
$0.0 \le f < 0.1$
0.2
0.3
0.4
0.5
0.6
0.7
0.8
0.9
1.0
$f = 1$
$p(d_{m,+1})$
0.00
0.02
0.04
0.06
80
85
90
95
100
105
Mobility Diameter $d_{m,+1}$ (nm)

Figure S4

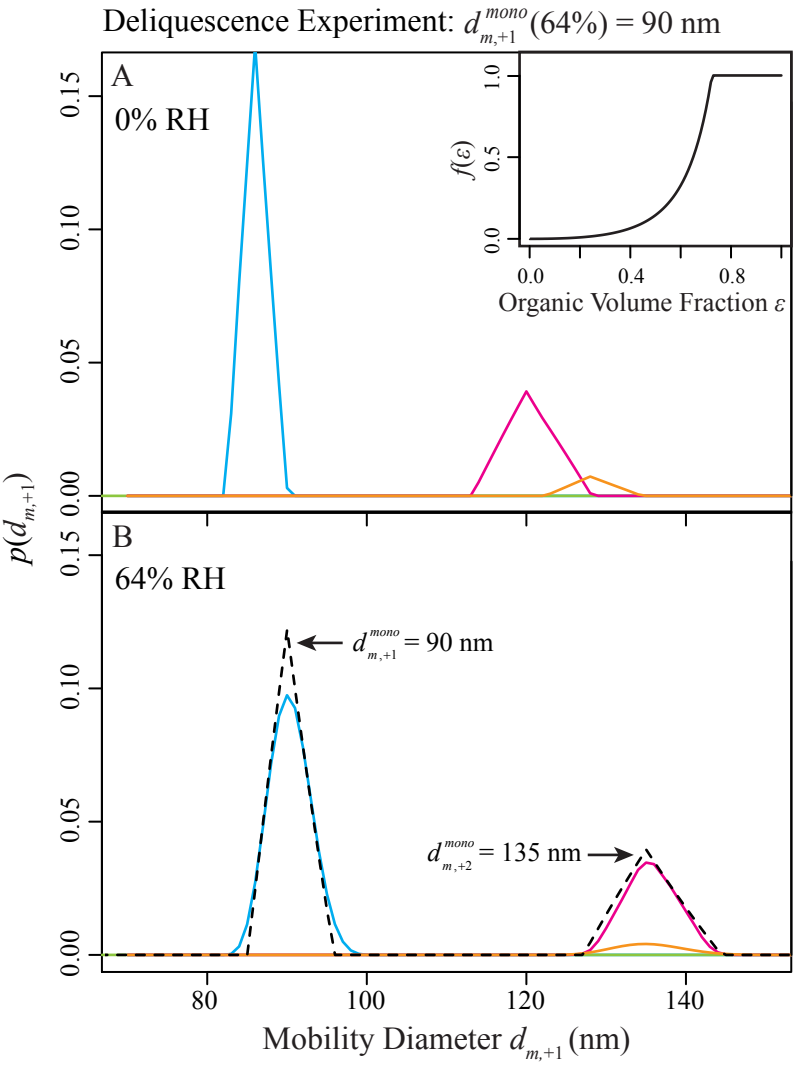
Deliquescence Experiment: $d_{m,+1}^{mono}$(64%) = 90 nm
A
0% RH
B
64% RH
$p(d_{m,+1})$
$f(\varepsilon)$
Organic Volume Fraction ε
$d_{m,+1}^{mono}$ = 90 nm
$d_{m,+2}^{mono}$ = 135 nm
Mobility Diameter $d_{m,+1}$ (nm)

Figure S5

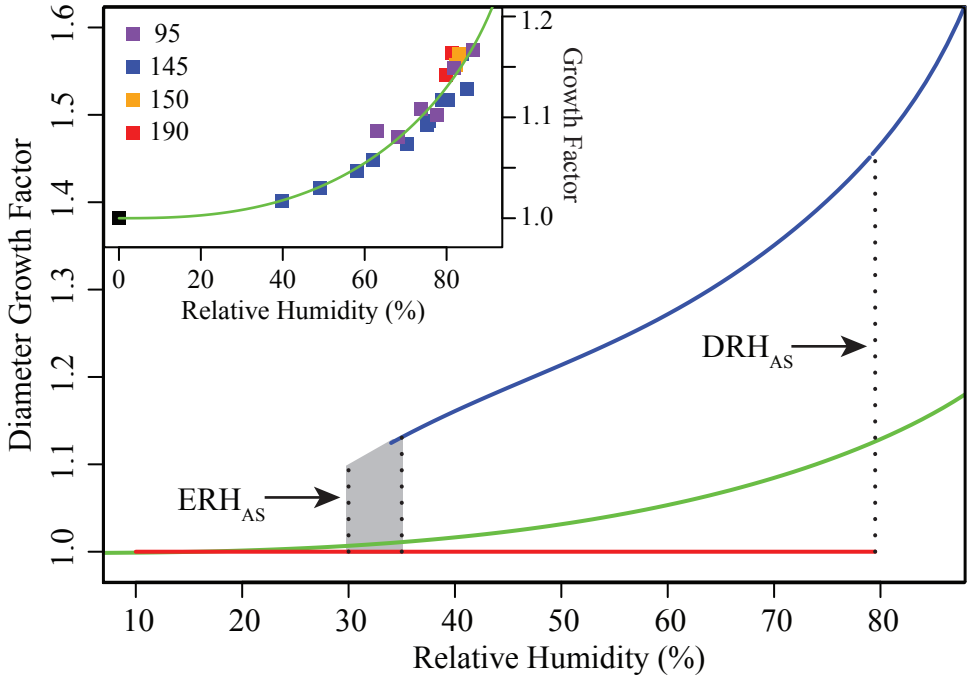
95
145
150
190
Growth Factor
Relative Humidity (%)
Diameter Growth Factor
ERH$_{AS}$
DRH$_{AS}$
Relative Humidity (%)

Figure S6

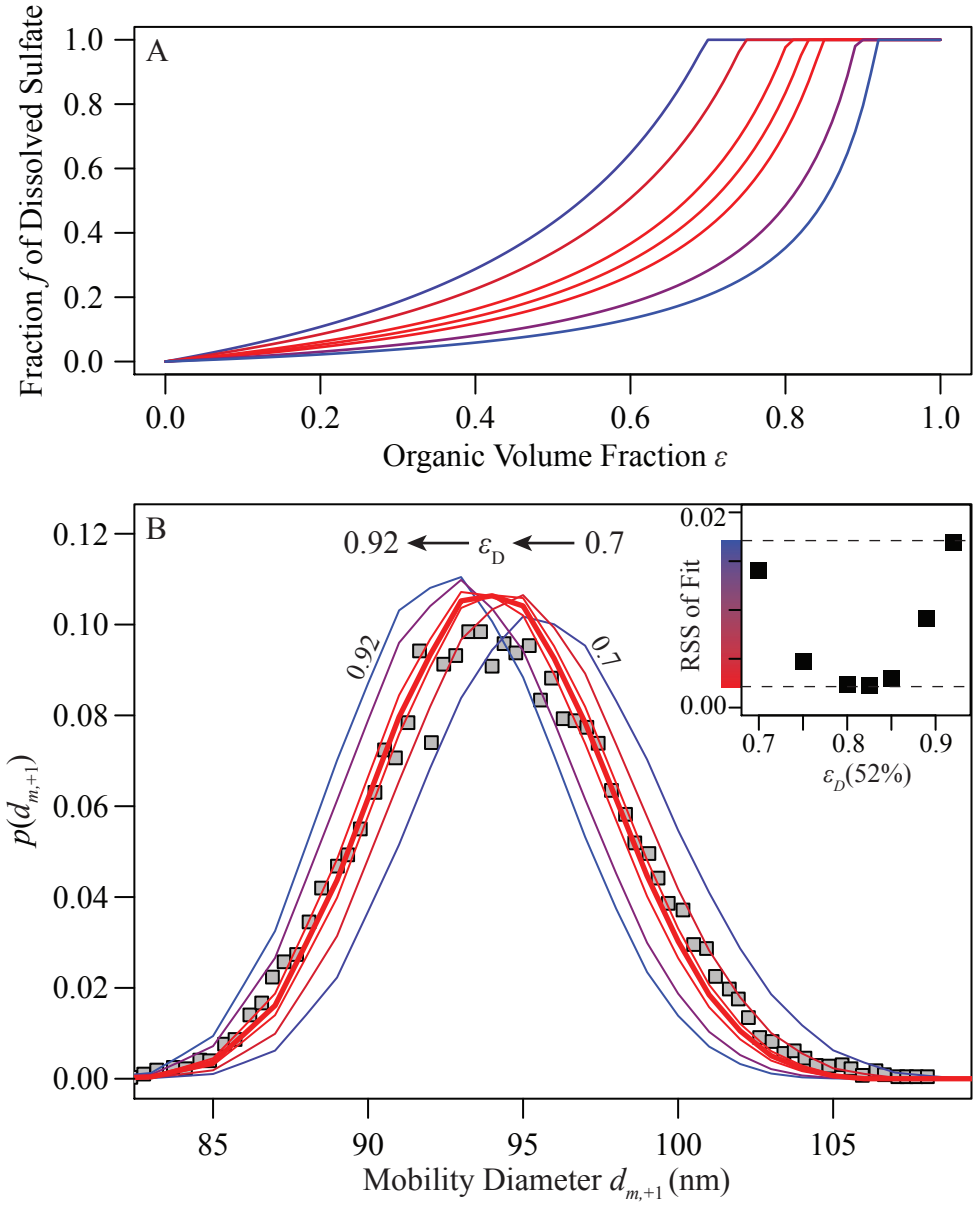
A
Fraction f of Dissolved Sulfate
1.0
0.8
0.6
0.4
0.2
0.0
0.0
0.2
0.4
0.6
0.8
1.0
Organic Volume Fraction ε
B
0.92 ← ε_D ← 0.7
0.92
0.7
$p(d_{m,+1})$
0.12
0.10
0.08
0.06
0.04
0.02
0.00
85
90
95
100
105
Mobility Diameter $d_{m,+1}$ (nm)
RSS of Fit
0.02
0.00
0.7
0.8
0.9
ε_D(52%)

Figure S7